# Energy Management for a Port Integrated Energy System Based on Distributed Dual Decomposition Mixed Integer Linear Programming

Teng, Fei; Zhang, Qing; Xiao, Geyang; Ban, Zixiao; Liang, Yuan; Guan, Yajuan

*Published in:*
Journal of Marine Science and Engineering

*DOI (link to publication from Publisher):*
10.3390/jmse11061137



*Publication date:*
2023

*Document Version*
Publisher's PDF, also known as Version of record

Journal of *Marine Science and Engineering*

MDPI

*Article*

# Energy Management for a Port Integrated Energy System Based on Distributed Dual Decomposition Mixed Integer Linear Programming

**Fei Teng [1], Qing Zhang [1], Geyang Xiao [2,*], Zixiao Ban [1], Yuan Liang [2] and Yajuan Guan[3]**

[1] Marine Electrical Engineering College, Dalian Maritime University, Dalian 116026, China; brenda_teng@163.com (F.T.); zq1120211224@dlmu.edu.cn (Q.Z.); bzx@dlmu.edu.cn (Z.B.)
[2] Research Institute of Intelligent Networks, Zhejiang Lab, Hangzhou 311121, China; liangyuan@zhejianglab.com
[3] Department of Energy, Aalborg University, 9220 Aalborg, Denmark; ygu@energy.aau.dk
* Correspondence: xgyalan@outlook.com

**Abstract:** This paper proposes a distributed energy management strategy, based on dual decomposition mixed integer linear programming for port integrated energy systems (PIESs), to improve the utilization of renewable energy, and to foster green ports. Firstly, due to the distributed characteristics presented by various heterogeneous devices, a polymorphic network-based PIES was established, instead of the traditional single IP protocol, incorporating electricity replacement and energy conversion devices. Secondly, taking into account the coupling of various energy flows, an energy management model was constructed, to ensure reliable operation for the PIES. Thirdly, an energy management strategy based on distributed dual decomposition mixed integer linear programming for the PIES was proposed, which took into account the distributed characteristic of the PIES. Finally, the effectiveness of the proposed strategy was demonstrated, by simulation cases in different scenarios for the PIES. The obtained energy management results were similar to the centralized algorithm.

**Keywords:** port integrated energy system (PIES); distributed energy management; mixed integer linear programming; polymorphic network



**Citation:** Teng, F.; Zhang, Q.; Xiao, G.; Ban, Z.; Liang, Y.; Guan, Y. Energy Management for a Port Integrated Energy System Based on Distributed Dual Decomposition Mixed Integer Linear Programming. *J. Mar. Sci. Eng.* **2023**, *11*, 1137. https://doi.org/10.3390/jmse11061137

Academic Editor: Claudio Ferrari

Received: 27 April 2023
Revised: 24 May 2023
Accepted: 26 May 2023
Published: 29 May 2023



## 1. Introduction

To accelerate the development of renewable energy, and to foster green seaports [1], innovative techniques of energy supply and energy conversion are being researched, aimed at improving energy efficiency, including Combined Cooling, Heating and Power (CCHP) [2] and electricity replacement devices [3]. Establishing a port integrated energy system (PIES) has become an urgent issue.

A PIES integrates energy supply devices, energy conversion devices, and energy consumption devices, including electricity, gas, heat, and cold multiple energy sources [4]. Many researchers have focused on the construction of PIESs. For instance, Ref. [5] explored the application of Bayesian networks to the integrated energy efficiency of ship–port interface. Ref. [6] suggested using modern control technologies and renewable energy sources to manage and operate a seaport lighting system efficiently. Ref. [7] provided a framework for an intelligent energy system, to ensure efficient and sustainable energy use in ports. Ref. [8] proposed a new integration scheme for a PIES, to achieve coordinated control and management between cold ironing and renewable sources. To reduce operating costs, Ref. [9] considered the use of hybrid-propulsion ships in seaports. Previous studies have only focused on partial devices of PIESs, but a seaport integrates multiple forms of energy, and contains various heterogeneous devices. To realize the coupling of multiple heterogeneous devices, establishing a PIES with more diverse electricity replacement devices and energy conversion devices has become an essential issue. Various devices,

such as CCHP, Electric Heater (EH), Electric Chiller (EC), Gas Boiler (GB) [10], Absorption Chiller (AC) [11], and Plug-in Electric Ship (PES) [12] have been integrated into PIESs by different manufacturers, and use different communication protocols. The devices exhibit different modalities, based on location and identity, and a polymorphic network needs to be constructed for supporting exchange information between different devices [13]. The polymorphic network includes advanced addressing and routing functional components, enabling the integration and cooperation of various modes, such as Internet Protocol (IP), content, identity, and geonetworking identification [14,15]. This flexible and efficient functional form of polymorphic network can adapt well to PIESs.

During the development of PIESs, many fundamental problems needed to be solved. To improve seaport energy efficiency, and to ensure the stability of PIESs, the energy management problem of PIESs is the key problem. To maintain seaport sustainability, Ref. [16] considered carbon emission constraints and energy conversion efficiency, so as to minimize the cost of electrical energy for ships. Ref. [17] proposed a green seaport model based on renewable energy, to achieve self-sufficiency and energy dispatch in seaports. Ref. [18] considered charging safety and battery life constraints, to minimize charging costs, and to improve the efficiency of electric boats. Ref. [19] presented an energy management model, to investigate the energy consumption and environmental impact of fishing vessels at different stages. To handle supply and demand balance constraints, Ref. [20] presented a multi-objective optimization model, to achieve optimal scheduling of the seaport. Ref. [21] presented an energy management model, to optimize the economic and reliability performance of hybrid renewable energy systems. Ref. [22] took into consideration constraints such as the output power of generating devices and the charging needs of electric vehicles, to minimize the overall cost. However, these studies only considered the energy management problem of partial devices, neglecting comprehensive and collaborative research on the energy management of entire PIESs.

The energy management challenge is to minimize the total cost, involving various constraints, such as the balance of supply and demand. To address this energy management problem, various centralized algorithms have been proposed [23–25]. However, these algorithms may result in single-point failures [26], less privacy [27], and increasing computational burdens. Additionally, due to the distributed characteristics of PIESs, heterogeneous devices require an appropriate distributed energy management strategy. Research on distributed algorithms has attracted the extensive attention of scholars. For example, Ref. [28] suggested a distributed sub-gradient algorithm for optimizing multi-agent systems. A distributed algorithm based on a multi-objective genetic algorithm for solving the technical and economic problems of microgrids was introduced in Ref. [29]. A distributed demand response market clearing algorithm was presented, together with an ideal cloud resource allocation, to spread the necessary processing resources, in Ref. [30]. To achieve the market commitments, a unique home energy management system control algorithm was employed in Ref. [31]. To solve the energy management problem, an exploration–exploitation balanced metaheuristic algorithm, based on inertia weight local search, was presented in Ref. [32]. The limited-communication distributed model predictive control algorithm was modified, to support grid-interactive buildings, in Ref. [33]. Ref. [34] proposed a distributed algorithm based on game theory, for optimal coalition formation and maximum profit allocation of distributed energy resources in smart grids. Ref. [35] recommended a distributed optimal energy management algorithm, to maintain the overall stability and reliability of the energy internet system. To obtain optimal solutions for PIESs, a fully dynamic-weighted coefficients distributed algorithm was presented in Ref. [36]. However, the PIES energy management problem is a mixed integer linear programming problem with coupling constraints, and the previous proposed algorithms are not applicable.

The main aim of this paper was to propose a distributed energy management strategy, based on the dual decomposition mixed integer linear programming algorithm

for PIESs, to improve energy efficiency. The innovative contributions of this paper are summarized below:

(1) A PIES based on a polymorphic network was constructed, to incorporate diverse heterogeneous seaport devices, and to enhance energy utilization efficiency. Due to the characteristics of the various heterogeneous devices, a polymorphic network-based PIES was established, which included electricity replacement devices and energy conversion devices.

(2) An energy management strategy based on distributed dual decomposition mixed integer linear programming for PIESs is proposed, to ensure reliable seaport operation. Considering the distributed characteristics of the various heterogeneous devices in PIESs, an energy management strategy based on distributed dual decomposition mixed integer linear programming is proposed, to solve the energy management problem, which is a mixed integer linear programming problem with coupling constraints.

The remainder of this paper is organized as shown in Figure 1. Section 2 describes the structure of a polymorphic network-based port integrated energy system (PIES) and the devices in the PIES. An energy management model for the PIES, and an energy management strategy based on dual decomposition mixed integer linear programming, are presented in Section 3. In Section 4, the effectiveness of the proposed energy management strategy in different scenarios is verified by numerical cases. Section 5 concludes the paper. The appendix contains some abbreviations that are covered in the paper.

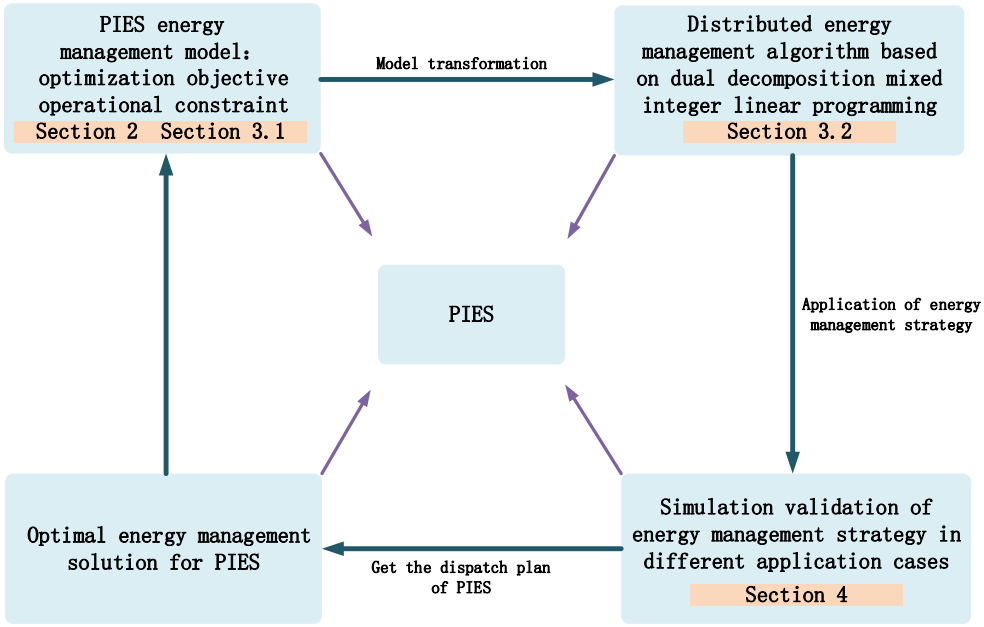


**Figure 1.** Node classification.

## 2. Structure of Port Integrated Energy System

For this section, a PIES was established, based on a polymorphic network, to incorporate various heterogeneous devices, depicted in Figure 2. The PIES comprised N Energy Bodies (EBs), consisting of various devices, including CCHP, EH, EC, Wind Turbine (WT), GB, AC, and PES. The CCHP device served as the energy conversion center, providing cold, heat, and electricity to the seaport. The EH and EC devices were crucial for promoting a sustainable and environmentally friendly energy structure, because they served as the electricity replacement devices. To implement intelligent control of different nodes, a polymorphic network was applied, to support communication between the heterogeneous devices.

The polymorphic network was intelligent, and played a critical role in the PIES. It consisted of a data layer, a control layer, and a service layer [37]. Specifically, the data

layer connected the physical devices of the PIES, including various sensors and actuators, and provided real-time device status information to the control layer. The control layer in the polymorphic network undertook addressing and routing between modalities such as content, IP, and geonetworking, controlling the data layer, to convert requirements and control information. The service layer of the polymorphic network focused on realizing the distributed energy management of the PIES: this layer was responsible for managing energy generation, distribution, and consumption across the entire network.

The structure of the PIES was as follows:

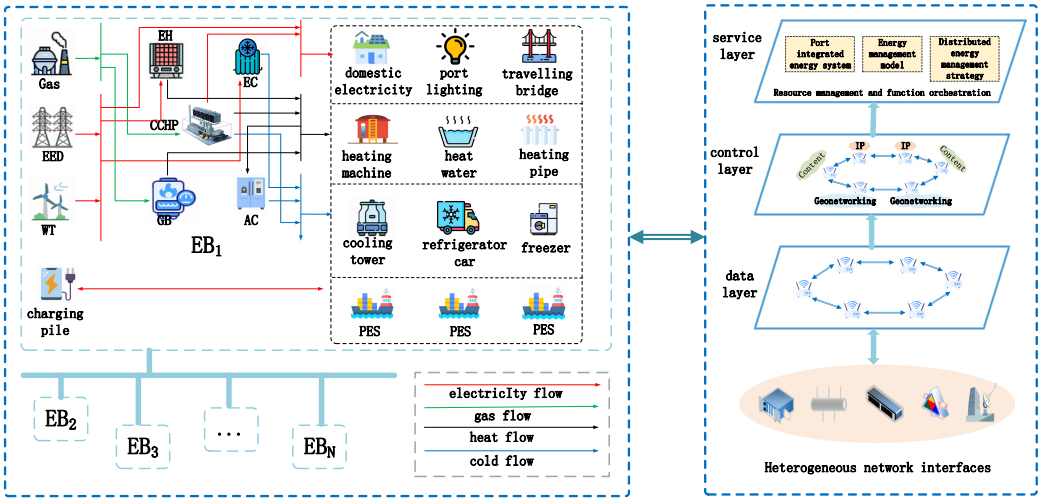


**Figure 2.** Node classification.

### 2.1. CCHP

A CCHP device is a crucial energy conversion device in PIESs, utilizing natural gas to provide an energy supply of cold, heat, and electricity.

The cost function for a CCHP device can be expressed as follows:

$$C^n_{CCHP} = C^n_{CCHP-E} + C^n_{CCHP-H} + C^n_{CCHP-L} \tag{1}$$

where the costs of electricity, heat, and cold production are represented by $C^n_{CCHP-E}$, $C^n_{CCHP-H}$, and $C^n_{CCHP-L}$ for the nth EB, respectively. The unit of these costs is CNY (Chinese Yuan); $n$ is the number of EBs.

More specifically, the costs of the electricity, heat, and cold production for a CCHP device can be expressed as follows:

$$C^n_{CCHP-E} = \sum_{t=1}^{T} c_g Q_{CCHP-E}(t) \tag{2}$$

$$C^n_{CCHP-H} = \sum_{t=1}^{T} c_g Q_{CCHP-H}(t) \tag{3}$$

$$C^n_{CCHP-L} = \sum_{t=1}^{T} c_g Q_{CCHP-L}(t) \tag{4}$$

where the amount of natural gas consumed by the CCHP device, to produce electricity, heat, and cold at time step t for the nth EB, is represented by $Q_{CCHP-E}(t)$, $Q_{CCHP-H}(t)$, and $Q_{CCHP-L}(t)$, respectively; the unit is $m^3$. The price of gas energy is represented by $c_g$, with a unit of CNY/$m^3$.

The energy conversion relationship of a CCHP device is stated as follows:

$$P^n_{CCHP}(t) = \eta_{CCHP-E} Q^n_{CCHP-E}(t) \tag{5}$$
$$H^n_{CCHP}(t) = \eta_{CCHP-H} Q^n_{CCHP-H}(t) \tag{6}$$
$$L^n_{CCHP}(t) = \eta_{CCHP-L} Q^n_{CCHP-L}(t) \tag{7}$$

where $P^n_{CCHP}(t)$ represents the electricity generated by the CCHP device for the nth EB at time step t, and $H^n_{CCHP}(t)$ and $L^n_{CCHP}(t)$ represent, respectively, the heat and cooling supplied by the CCHP device for the nth EB at time step t; the unit is kW; $\eta_{CCHP-E}$, $\eta_{CCHP-H}$, and $\eta_{CCHP-L}$ are the conversion efficiencies of electricity, heat, and cold, respectively.

To ensure safety, a CCHP device has to comply with the following constraints:

$$0 \le P^n_{CCHP}(t) \le P^{max}_{CCHP} \tag{8}$$
$$0 \le H^n_{CCHP}(t) \le H^{max}_{CCHP} \tag{9}$$
$$0 \le L^n_{CCHP}(t) \le L^{max}_{CCHP} \tag{10}$$

where $P^{max}_{CCHP}$, $H^{max}_{CCHP}$, and $H^{max}_{CCHP}$ are, respectively, the maximum electricity, heat, and cold output by the CCHP device for the nth EB at time step t; the unit is kW.

### *2.2. WT*

A WT is a critical device for generating electricity from wind energy, and reducing environmental pollution. To ensure its safe operation, the following constraint must be met:

$$0 \le P^n_{WT}(t) \le P^{max}_{WT}, \tag{11}$$

where the electricity output of the WT, denoted by $P^n_{WT}(t)$ at time t in the nth EB, should be between 0 and $P^{max}_{WT}$, which indicates the WT's maximum electricity output; the unit is kW.

### *2.3. External Electricity Device (EED)*

To address the high electricity demand of our PIES, we incorporated an EED that could directly purchase electricity from the power grid. The cost of electricity consumption for an EED in the nth EB can be calculated by the following:

$$C^n_{EED} = \sum_{t=1}^{T} c_e P^n_{EED}(t), \tag{12}$$

where $C^n_{EED}$ is the cost of the electricity consumption of the EED in the nth EB, and the unit is $CNY$; $c_e$ is the time-of-use tariff, and the unit is CNY/kWh.

It is important to note that the electricity consumption of the EED, denoted as $P^p_{EED}(t)$, must adhere to the following constraints:

$$0 \le P^{\mathrm{n}}_{EED}(t) \le P^{max}_{EED}, \tag{13}$$

where $P^n_{EED}(t)$ is the electricity consumption of the EED in the nth EB at time t, and the unit is $kW$; $P^{max}_{EED}$ is the maximum electricity consumption of the EED, and the unit is kW.

### *2.4. EH*

An EH device's basic principle is to produce heat by utilizing electricity, and its cost function corresponds to the following:

$$C^n_{EH} = \sum_{t=1}^{T} c_e P^n_{EH}(t), \tag{14}$$

where $C_{EH}^{n}$ is the cost of the electricity consumption of the EH device in the nth EB, and the unit is CNY; $P_{EH}^{n}(t)$ is the electricity consumption of the EH device in the nth EB at time t, and the unit is kW.

The EH device's energy conversion relationship is as follows:

$$H_{EH}^{n}(t) = \eta_{EH} P_{EH}^{n}(t), \tag{15}$$

where $H_{EH}^{n}(t)$ denotes the amount of heat the EH device produces at time t in the nth EB, and the unit is kW.

To reduce the EH failure rate, the following constraints need to be observed:

$$0 \leq H_{EH}^{n}(t) \leq H_{EH}^{max}, \tag{16}$$

where $H_{EH}^{max}$ is the maximum heat output of EH, and the unit is kW.

### 2.5. GB

GB devices are commonly used for heat production by burning natural gas. The total cost of gas consumption by the GB device in the nth EB is represented by $C_{GB}^{n}$, which is calculated as follows:

$$C_{GB}^{n} = \sum_{t=1}^{T} c_g Q_{GB}^{n}(t), \tag{17}$$

where $C_{GB}^{n}$ is the total cost of gas consumption by the GB device in the nth EB, and the unit is $CNY$; $Q_{GB}^{n}(t)$ is the gas consumption of GB in the nth EB at time t, and the unit is $m^3$.

To display the working principle of the GB device, its energy conversion relationship can be described as follows:

$$H_{GB}^{n}(t) = \eta_{GB} Q_{GB}^{n}(t), \tag{18}$$

where $H_{GB}^{n}(t)$, $\eta_{GB}$, and $Q_{GB}^{n}(t)$ represent the heat output, heat efficiency, and gas consumption, respectively, of the GB device in the nth EB. The unit of $H_{GB}^{n}(t)$is $kW$, and the unit $Q_{GB}^{n}(t)$ is $m^3$.

The following safety operating constraint was in effect, to guarantee safe and compliant activities:

$$0 \leq H_{GB}^{n}(t) \leq H_{GB}^{max}, \tag{19}$$

where $H_{GB}^{n}(t)$ and $H_{GB}^{max}$ denoted, respectively, the heat output and upper bound of the heat energy production capacity of the GB device in the $n$ EB at t period, and the unit was kW.

### 2.6. EC

Compared to conventional cold methods, an EC device offers higher cold efficiency and lower energy consumption. The cost function of an EC device is as follows:

$$C_{EC}^{n} = \sum_{t=1}^{T} c_e P_{EC}^{n}(t), \tag{20}$$

where $C_{EC}^{n}$ represents the total cost of electricity consumption of the EC device in the nth EB, and the unit is CNY; $P_{EC}^{n}(t)$ denotes the EC device's electricity consumption in the nth EB at time t, and the unit is kW.

The energy efficiency of the EC device can be defined as the ratio between the cold produced and the electricity consumed. The energy conversion relationship of the EC device is determined below:

$$L_{EC}^{n}(t) = \eta_{EC} P_{EC}^{n}(t), \tag{21}$$

where $L_{EC}^{n}(t)$ and $\eta_{EC}$ represent, respectively, the cold output and the cold efficiency of the EC device in the nth EB, and the unit of $L_{EC}^{n}(t)$ is kW.

For better control and management of the EC device, the following safety constraint needed to be satisfied:

$$0 \leq L_{EC}^{n}(t) \leq L_{EC}^{max}, \tag{22}$$

where $L_{EC}^{max}$ was the maximum heat output of the EC, and the unit was kW.

### 2.7. AC

An AC device utilizes absorbent, to absorb and release heat during evaporation and condensation processes, achieving cold in a low-temperature space. An AC device energy conversion relationship is as follows:

$$L_{AC}^{n}(t) = \eta_{AC} H_{AC}^{n}(t), \tag{23}$$

where $L_{AC}^{n}(t)$,$H_{AC}^{n}(t)$ and $\eta_{AC}$ denote, respectively, the cold output, heat input, and cold efficiency of the AC device in the nth EB. The unit of $L_{AC}^{n}(t)$ and $H_{AC}^{n}(t)$ is kW.

To avoid possible accidents with an AC device, the following safety constraint needs to be met:

$$0 \leq L_{AC}^{n}(t) \leq L_{AC}^{max}, \tag{24}$$

where $L_{AC}^{max}$ denotes the maximum cold output of the AC device, and the unit is kW.

### 2.8. PES

A PES uses batteries as its power source in a seaport. Compared to traditional fuel ships, a PES has the advantage of being more environmentally friendly and energy efficient. A PES can also reduce pollution, and improve comfort and safety during navigation; its operating constraints can be described as

$$e_n(0) = \mathrm{E}_n^{init}, \tag{25}$$

$$e_n(t+1) = e_n(t) + P_n \Delta T(\zeta_n^u \mathbf{u}_n(t) - \zeta_n^v \mathbf{v}_n(t)), k \in (0, ..., T-1), \tag{26}$$

$$e_n(T) \geq \mathrm{E}_n^{ref}, \tag{27}$$

$$\mathrm{E}_n^{min} \leq e_n(t) \leq \mathrm{E}_n^{max}, \tag{28}$$

$$u_n(t) + v_n(t) \leq 1, \tag{29}$$

where the initial energy storage is denoted by $\mathrm{E}_n^{init}$, and the energy storage at time $t+1$ is calculated based on the energy inputs and outputs at time $t$. The charging and discharging states are represented by $u_n(t)$ and $v_n(t)$, respectively. The energy storage at time $T$ must be greater than or equal to the reference energy $\mathrm{E}_n^{ref}$, while the energy storage at any time must be within the range of minimum energy $\mathrm{E}_n^{min}$ and maximum energy $\mathrm{E}_n^{max}$. These constraints ensure that the PES operates within the specified energy range, and meets the required energy demands. The unit of $\mathrm{E}_n^{init}$, $\mathrm{E}_n^{ref}$, $\mathrm{E}_n^{min}$, and $\mathrm{E}_n^{max}$ is kWh.

## 3. Energy Management Strategy for Port Integrated Energy System

For this section, an energy management model for our PIES was constructed, to improve its energy efficiency and economic benefit. An energy management strategy based on distributed dual decomposition mixed integer linear programming was proposed, to solve the energy management problem.

### 3.1. Energy Management Model

An energy management model for our PIES was established, to minimize the operation cost, consisting of the following objective functions and constraints.

#### 3.1.1. Objective Function

The objective function for our PIES was described as:

$$\boldsymbol{min} \quad C_{total} = \sum_{n=1}^{N} C_E^n + C_G^n + C_{ship}^n, \tag{30}$$

where $C_{total}$ represented the total operating cost of the PIES, and N indicated the number of EBs. The objective function for each EB comprised three components: the cost of the purchased electricity ($C_E^n$); the cost of the purchased gas ($C_G^n$); and the cost of the PES ($C_{ship}^n$). The unit of these costs was the CNY.

(1) The cost of purchased electricity $C_E^n$:

$$C_E^n = C_{EED}^n + C_{EH}^n + C_{EC}^n, \tag{31}$$

where $C_E^n$ included the purchased cost of the EED ($C_{EED}^n$), the electricity purchased cost of the EH device ($C_{EH}^n$), and the electricity purchased cost of the EC device ($C_{EC}^n$). The unit of these costs was the CNY.

(2) The cost of purchased gas red $C_G^n$:

$$C_G^n = C_{CCHP}^n + C_{GB}^n, \tag{32}$$

where $C_G^n$ included the gas purchased cost of the CCHP device ($C_{CCHP}^n$), and the gas purchased cost of the GB device ($C_{GB}^n$). The unit of these costs was the CNY.

(3) The cost of a PES $C_{ship}^n$:

$$C_{ship}^n = \sum_{t=1}^{T} P^n(C^u(t)u^n(t) - C^v(t)v^n(t)), \tag{33}$$

where $C^u$ was the charging price, $C^v$ was the discharging price, and the unit was the CNY; $P^n$, $u^n(t)$, and $v^n(t)$ were utilized in this model, to indicate the charging and discharging power for each time period, as well as the corresponding charging and discharging states. The unit of $P^n$ was kW.

#### 3.1.2. Constraints

To ensure the energy supply security of a PIES, the following constraints should be followed.

(1) Safety operation constraints.

To prevent electricity accidents and other safety accidents, a PIES needs to have robust safety performance. The safety operation constraints of a PIES are divided into two parts: the general safety operation constraints of the seaport, and the safety operation constraints of each device:

$$\sum_{n=1}^{N}(P_{EED}^n(t) + P_{EH}^n(t) + P_{EC}^n(t)) \le P_{\max;} \tag{34}$$

$$\sum_{n=1}^{N}(Q_{CCHP-E}^n(t) + Q_{CCHP-H}^n(t) + Q_{CCHP-L}^n(t)) + Q_{GB}^n(t) \le Q_{\max;} \tag{35}$$

$$P^{min}(t) \le \sum_{n=1}^{N} P^n(u^n(t) - v^n(t)) \le P^{max}(t), \tag{36}$$

where $P_{\max}$ is the upper bound of the electricity purchased by all the devices in the PIES, $Q_{\max}$ is the upper bound of the gas purchased by all the devices in the PIES, and $P^{min}(t)$ and $P^{max}(t)$ are the lower and upper bounds, respectively, of the power output of all the PESs in the PIES at t period. The unit of $P_{\max}$, $Q_{\max}$, $P^{min}(t)$, and $P^{max}(t)$ is kW.

The safety operation constraints for various devices in a PIES are described in Section 2.

(2) Supply and demand balance constraints.

To meet the energy requirements of the different users in a PIES, it is necessary to maintain the balance between energy supply and demand.

Electricity supply and demand balance constraint:

$$P^n_{CCHP}(t) + P^n_{EED}(t) + P^n_{WT}(t) = P^n_{load}(t), \tag{37}$$

where $P^n_{load}(t)$ is the electricity load of each EB device in the PIES at t period, and the unit is kW.

Heat supply and demand balance constraint:

$$H^n_{CCHP}(t) + H^n_{EH}(t) + H^n_{GB}(t) = H^n_{load}(t), \tag{38}$$

where $H^n_{load}(t)$ is the heat load of each EB device in the PIES at t period, and the unit is kW.

Cold supply and demand balance constraint:

$$L^n_{CCHP}(t) + L^n_{EC}(t) + L^n_{AC}(t) = L^n_{load}(t); \tag{39}$$

where $L^n_{load}(t)$ is the cold load of each EB device in the PIES at t period, and the unit is kW.

In summary, Equations (1)–(39) constituted the energy management model for our PIES.

### *3.2. Distributed Dual Decomposition Mixed Integer Linear Programming Algorithm*

To address the energy management problem for our PIES, we proposed a distributed energy management strategy based on dual decomposition mixed integer linear programming [38], which was different from the previous centralized energy management strategy [23–25], and was more suitable for the distributed characteristics of a port. As our PIES was a multi-energy flow system coupled with electricity, cold, and heat, we converted the model, i.e., Equations (1)–(39), to Equation (40), before designing the distributed energy management strategy.

A PIES is a Multi-Agent System (MAS) comprised of various nodes, and the communication network must satisfy specific conditions. The communication network topology utilized by a PIES is illustrated in the form of a directed graph, represented by $G = (V, E_k)$. The graph's nodes($V = 1, \ldots, I$) stand in for many agents interacting with the system, and the set of directed edges ($E_k$) is determined by the formula: $E_k = (j, i) : a_j i(k) > 0$.

If $a^i_j(k) > 0$ for any $i, j \in 1, \ldots, I$ and $k \geq 0$, then it follows that $a^i_j(k) \geq \eta$ and $a^i_i(k) \geq \eta$, where $\eta$ is a constant within the range of (0,1). Additionally, for all $k \geq 0$: (1) $\sum_{j=1}^{I} a^i_j(k) = 1$ for every $i \in 1, \ldots, I$; and (2) $\sum_{i=1}^{I} a^i_j(k) = 1$ for every $j \in 1, \ldots, I$. The graph $G(V, E_\infty)$ satisfies strong connectivity, implying that there exists a directed path of edges linking any two nodes within the graph. Additionally, there exists a positive integer $T \geq 1$, such that for every edge $(j, i) \in E_\infty$, agent $i$ receives information from a neighboring agent $j$ at least once every $T$ consecutive iterations.

$$
\begin{cases}
\min \quad \sum_{i_e=1}^{I_E}\left(C_{CCHP-E}+C_{EED}\right)+\sum_{i_h=1}^{I_H}\left(C_{CCHP-H}+C_{EH}+C_{GB}\right)+\sum_{i_l=1}^{I_L}\left(C_{CCHP-L}+C_{EC}\right)+\sum_{i_{ship}=1}^{I_{ship}} C_{ship} \\
\text{s.t} \quad \begin{cases}
\sum_{i_e=1}^{I_E} P_{EED}^{n}(t)+\sum_{i_h=1}^{I_H} P_{EH}^{n}(t)+\sum_{i_l=1}^{I_L} P_{EC}^{n}(t) \le P_{\max} \\
\sum_{i_e=1}^{I_E} Q_{CCHP-E}^{n}(t)+\sum_{i_h=1}^{I_H} Q_{CCHP-H}^{n}(t)+\sum_{i_l=1}^{I_L} Q_{CCHP-L}^{n}(t)+\sum_{i_h=1}^{I_H} Q_{GB}^{n}(t) \le Q_{\max} \\
P^{\min} \le \sum_{i_{ship}=1}^{I_{ship}} P^{n}\left(u^{n}-v^{n}\right) \le P^{\max}
\end{cases} \\
Y=Y_e \cup Y_h \cup Y_l \cup Y_{ship} \\
\begin{cases}
Y_e^n=\left\{\begin{bmatrix} P_{CCHP}^{n}(t) \\ P_{EED}^{n}(t) \\ P_{WT}^{n}(t) \end{bmatrix} \in R^{NT}(t=1,\ldots,T \ \ and \ \ n=1,\ldots,N) | \text{Eq.}(1)(4)(11)-(12)\right\} \\
Y_h^n=\left\{\begin{bmatrix} H_{CCHP}^{n}(t) \\ H_{EH}^{n}(t) \\ H_{GB}^{n}(t) \end{bmatrix} \in R^{NT}(t=1,\ldots,T \ \ and \ \ n=1,\ldots,N) | \text{Eq.}(2)(5)(14)-(15)(17)-(18)\right\} \\
Y_l^n=\left\{\begin{bmatrix} L_{CCHP}^{n}(t) \\ L_{EC}^{n}(t) \\ L_{AC}^{n}(t) \end{bmatrix} \in R^{NT}(t=1,\ldots,T \ \ and \ \ n=1,\ldots,N) | \text{Eq.}(3)(6)(20)-(21)(23)-(24)\right\} \\
Y_{ship}^n=\left\{\begin{bmatrix} e^{n}(t) \\ u^{n}(t) \\ v^{n}(t) \end{bmatrix} \in R^{NT}(t=1,\ldots,T \ \ and \ \ n=1,\ldots,N) | \text{Eq.}(25)-(29)\right\}
\end{cases}
\end{cases}
\tag{40}
$$

As mentioned above, we constructed a communication network consisting of 12 nodes, including 3 electricity nodes, 3 heat nodes, 3 cold nodes and 3 PES nodes. Note that the described conditions required the adjacency matrix of the 12 nodes to be updated once every two iterations: we chose one of the figures which satisfied the conditions, as shown in Figure 3.

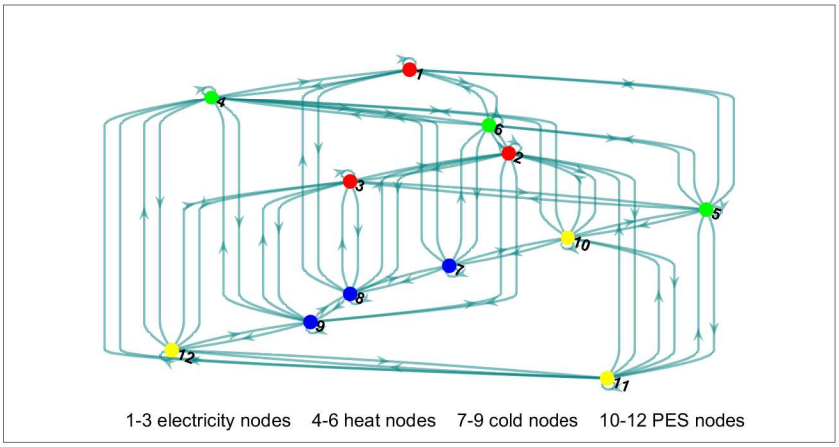


**Figure 3.** Node classification.

The energy management problem for our PIES was a mixed integer linear programming problem, containing both global coupling and local constraints. The optimization problem could be redefined as (40), where $I_E$ denoted the number of electricity nodes, $I_H$ represented the number of heat nodes, $I_L$ signified the number of cold nodes, and $I_{ship}$ corresponded to the number of PES nodes. Additionally, $Y_e$ was the set of electricity nodes, $Y_h$ denoted the set of heat nodes, $Y_l$ represented the set of cold nodes, and $Y_{ship}$ stood for the set of PES nodes. $Y$ referred to the set of all decision variables.

Our PIES energy management problem was defined as (41) and (42):

$$\min_{\{y_i \in y_i\}_{i=1}^{I}} \sum_{i \in I} c_i^T y_i \tag{41}$$

$$\sum_{i=1}^{I} A_i y_i \leq b, \tag{42}$$

where $I$ was the number of nodes, and the cost function corresponding to node $i$ was represented by $c_i^T y_i$, where $y_i$ denoted the output of node $i$ [38].

The Lagrangian function for this problem could be represented as (44), where $y = [y_1^\top \dots y_I^\top]^\top \in Y = Y_1 \times \cdots \times Y_I \subseteq \mathbb{R}^n$ with $n = \sum_{i=1}^{I} NT$, $\lambda \in \mathbb{R}_+^{4T}$ was the vector of Lagrange multipliers:

$$L(y, \lambda) = \sum_{i=1}^{I} L_i(y_i, \lambda) = \sum_{i=1}^{I} \Big( c_i^T y_i + \lambda^T (A_i y_i - b) \Big). \tag{43}$$

Expressed mathematically, the dual function took on the following form:

$$d(\lambda) \doteq \min_{y \in Y} L(y, \lambda). \tag{44}$$

Because the dual function was divisible, the dual function could be described as:

$$d(\lambda) = \sum_{i=1}^{I} d_i(\lambda) = \sum_{i=1}^{I} \min_{y_i \in Y_i} L_i(y_i, \lambda). \tag{45}$$

The dual problem could be formulated as follows:

$$\mathcal{D} : \max_{\lambda \geq 0} \sum_{i=1}^{I} d_i(\lambda). \tag{46}$$

We made the following assumptions, before designing the solution algorithm.

**Assumption 1.** *For $i$ in the range of 1 to $I$, both the function $c_i^T y_i : \mathbb{R}^{NT} \to \mathbb{R}$ and each component of $A_i y_i - b$ are convex. Additionally, for all $i$ in the range of 1 to $I$, the set $Y_i \subseteq \mathbb{R}^{NT}$ is also convex.*

**Assumption 2.** *For each $i$ within the range of 1 to $I$, the set $Y_i$ is a compact subset of $\mathbb{R}^{NT}$.*

**Assumption 3.** *There is a vector $\tilde{y} = [\tilde{y}_1 \dots \tilde{y}_I]^\top \in relint(Y)$, where $relint(Y)$ represents the relative interior of the set $Y$. Moreover, it holds true that $\sum_{i=1}^{I} A_i \tilde{y}_i - b \leq 0$ for any components of $\sum_{i=1}^{I} A_i \tilde{y}_i - b$ that are linear in $y$, while $\sum_{i=1}^{I} A_i \tilde{y}_i - b < 0$ for all other components.*

If **Assumptions 1–3** are satisfied, there is strong duality and there exists an optimal primal–dual pair $(y^\star, \lambda^\star)$, where $y^\star = [y_1^\star \dots y_I^\star]^\top$. Additionally, we have:

$$L(y^\star, \lambda) \leq L(y^\star, \lambda^\star) \leq L(y, \lambda^\star), \lambda \in \mathbb{R}_+^{NT}, y \in Y. \tag{47}$$

**Assumption 4.** *Suppose that $\{c(k)\}_{k \geq 0}$ is a sequence of positive real numbers that decreases monotonically, and satisfies the condition $c(k) \leq c(r)$ for all $k \geq r \geq 0$: (1) $\sum_{k=0}^{\infty} c(k) = \infty$; and (2) $\sum_{k=0}^{\infty} c(k)^2 < \infty$, where $c(k) = \beta/(k+1)$ is a positive value for $\beta$.*

Therefore, we applied a distributed dual decomposition mixed integer linear programming algorithm [38], as shown in Algorithm 1.

**Algorithm 1** Distributed dual decomposition mixed integer linear programming algorithm

**Initialization** :
$k = 0$.
Consider $\hat{y}_i(0) \in Y_i$, for all $i = 1, \ldots, I$.
Consider $\lambda_i(\mathbf{0}) \in \mathbb{R}_+^{4T}$, for all $i = 1, \ldots, I$.
**while** not converged **do**
  **for** $i = 1, \ldots, m$ **do**
    $l_i = \sum_{j=1}^{I} \mathrm{a}_j^i \lambda_j$
    $y_i[k+1] \in \arg\min_y (c_i^T y_i + l_i^T A_i y_i - l_i^T \frac{b}{I})$
    $\lambda_i[k+1] = [0, l_i + c_k A_i y_i[k+1] - c_k \frac{b}{I}]^+$
    $\hat{y}_i[k+1] = \frac{\left[\sum_{r=0}^{k-1} c_r y_{ir}\right] + c_k y_i[k+1]}{\left[\sum_{r=0}^{k-1} c_r\right] + c_k}$
  **end for**
  $k \leftarrow k+1$.
**end while**

In Algorithm 1, we used two different sequences, $\hat{y}i(k)$ and $\tilde{y}i(k)$, to correct $yi(k)$, rendering the obtained solution closer to the real solution. The sequence $\hat{y}i(k)$ was the one-step-ahead forecast of $yi(k)$ from the previous iteration, while $\tilde{y}_i(k+1)$ was the weighted average of the previous observations and the one-step-ahead forecast: $\tilde{y}_i(k+1) = \begin{cases} \hat{y}_i(k+1) & k < k_{s,i} \\ \frac{\sum_{r=k_{s,i}}^{k} c(r) y_i(r+1)}{\sum_{r=k_{s,i}}^{k} c(r)} & k \geq k_{s,i} \end{cases}$, where $c(k) = \frac{0.1}{k+1}$ was the weight function.

In summary, the optimal solution for the energy management problem could be obtained by Algorithm 1.

## 4. Numerical Results

For this section, the effectiveness of our distributed energy management strategy based on dual decomposition mixed integer linear programming was verified for our PIES. The operation parameters of the simulation are shown in Tables 1 and 2, where Table 1 shows the parameters of the different devices, and Table 2 shows the time-of-use tariff.

To improve energy efficiency and reduce operational costs, two different strategies were applied, for solving the energy management problem of our PIES constructed by Equations (1)–(39). Case 1 was solved by a centralized algorithm, while Case 2–4 used the proposed strategy outlined in Section 3. The details of each case are explained below.

Case 1: According to the multi-energy flow coupling of our PIES, different kinds of heterogeneous devices, such as WT, CCHP, GB were integrated into the PIES, which contained different device operation constraints, and utilized intlinprog algorithm [39,40] to realize the energy management for the PIES on a typical summer day.

Case 2–4: Taking into account the differing characteristics of the various devices' outputs, we classified the nodes as shown in Figure 5. The classification problem was reformulated as Equation (40), and the further problem was transformed into Equations (41) and (42). Then, we applied the proposed strategy in Section 3, to solve the energy management problem for our PIES in different scenarios. Specifically, Case 2 was on a summer typical day, while Case 3 was on a typical winter day, and Case 4 was in the event of an equipment failure by the WT.

**Table 1.** Device parameter.

| Device Parameter | Numerical Value |
|---|---|
| $\eta_{CCHP-E}$ | 0.4 |
| $c_g$ | 0.35 (CNY/m$^3$) |
| $\eta_{CCHP-H}$ | 0.385 |
| $\eta_{EH}$ | 2.3 |
| $\eta_{GB}$ | 0.85 |
| $\eta_{CCHP-L}$ | 0.43 |
| $\eta_{EC}$ | 2.9 |
| $\eta_{AC}$ | 0.7 |
| $P_{CCHP}^{max}$ | 250 (kW) |
| $P_{EED}^{max}$ | 100 (kW) |
| $H_{CCHP}^{max}$ | 50 (kW) |
| $H_{EH}^{max}$ | 100 (kW) |
| $H_{GB}^{max}$ | 50 (kW) |
| $L_{AC}^{max}$ | 50 (kW) |
| $L_{CCHP}^{max}$ | 100 (kW) |
| $E_n^{min}$ | 1 (kWh) |
| $E_n^{max}$ | [8;16] (kWh) |
| $E_n^{init}$ | [0.2;0.5] $E_n^{max}$ (kWh) |
| $E_n^{ref}$ | [0.55;0.8] $E_n^{max}$ (kWh) |
| $\Delta T$ | 60 (min) |
| $P_n$ | [3;5] (kW) |
| $P^{max}$ | 9 (kW) |
| $P^{min}$ | −9 (kW) |
| $C^u$ | [0.6;1.1] (CNY/kWh) |
| $C^v$ | $1.1C^u$ (CNY/kWh) |
| $\zeta_n$ | [0.015;0.075] |

**Table 2.** Time-of-use tariff.

| Time Period | Electricity Price (CNY/kW) |
|---|---|
| 01:00–07:00 | 0.38 |
| 08:00–11:00 | 0.68 |
| 12:00–14:00 | 1.20 |
| 15:00–18:00 | 0.68 |
| 19:00–22:00 | 1.20 |
| 22:00–24:00 | 0.38 |

### *4.1. Case 1: Centralized Energy Management for PIES*

In this case, we considered an energy management problem for our PIES with 24-h dispatch, which included three (N = 3) EBs. Then, we applied the traditional centralized strategy to the energy management problem for our PIES on a typical summer day, implemented by intlinprog in matlab.

In the dispatch plan for the different energy flows, different devices could be supplied, with flexible and variable output power, depending on the load. The scheduling plans for the different energy flows of electricity, cold, and heat are given in Figure 4.

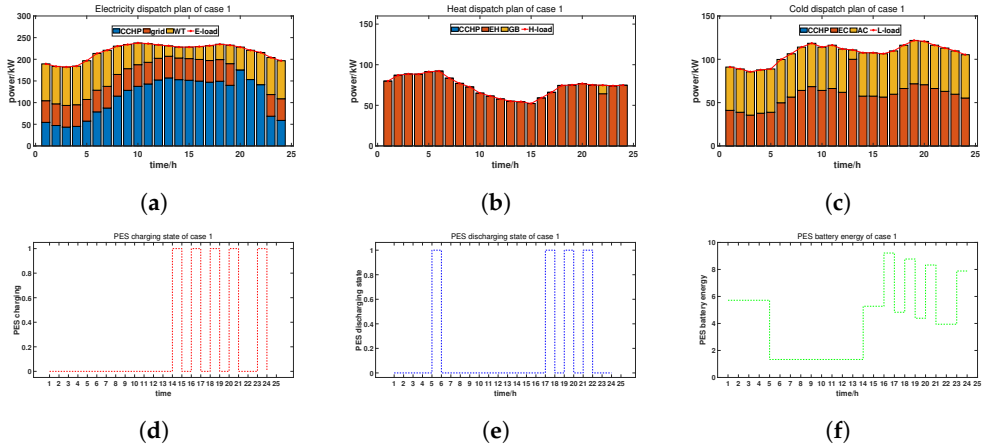


**Figure 4.** Dispatch plan of Case 1: (**a**) electricity dispatch plan; (**b**) heat dispatch plan; (**c**) cold dispatch plan; (**d**) PES charging state; (**e**) PES discharging state; (**f**) PES battery energy.

During periods of high electricity demand, the CCHP device was the main power generation device, and its output was stable at 114.99 kW to 175.53 kW, reaching a peak value of 128.34 kW around 8:00–9:00. The EED maintained a steady output of 50 kW throughout this period. The output of the WT gradually decreased from morning until late afternoon, fluctuating between 40 kW to 90 kW during peak hours. During low demand periods, the CCHP device output fluctuated around 43.45 kW to 58.91 kW, while the EED remained at a steady zero output. The WT output also fluctuated around 25.21 kW to 74.24 kW. In summary, the CCHP device was the main power generation device in the system, providing most of the electricity during peak demand periods. The EED acted as a backup power source, maintaining system stability. The WT, as a renewable energy source, provided a complementary power supply to the system, with high output during early morning and late afternoon, when the other sources were relatively weak.

In the heat dispatch plan, the output of the CCHP device remained at zero throughout 24 h, while the output of the EH device fluctuated during the same period: the highest value appeared at 5:00 (91.376 kW), and during the high load periods (from 15:00 to 18:00), its output remained above 70 kW. The GB device had no output from 1:00 to 21:00, with only a minimal output of 10.46 kW occurring at 22:00. It can be concluded that the EH device was the main power generation device, and played a crucial role in the operation of the system, while the GB and CCHP devices served as auxiliary backup devices. During the low load period, the output of all three devices was weak, but the EH device's output was still higher than that of the other two; therefore, the EH device played a critical role, while the GB and CCHP devices played a supporting role in the system.

In the cold dispatch plan, the CCHP device did not produce any output with a power value of 0. The output of the EC device fluctuated greatly during this period: during low load periods (1:00 and 20:00–24:00), the output decreased to around 35.56 kW; at 13:00, it reached 100 kW, while during high load periods (5:00–12:00 and 14:00–18:00), it stayed above 60 kW, with a peak of 71.76 kW. The AC device sustained a relatively stable output of 50 kW throughout the 24-h period, except in the 13th interval, where its output decreased to 10.79 kW. During cold load hours (5:00–12:00 and 14:00–18:00), the EC device maintained an output of over 70 kW, as the main power source, with the AC device playing a supporting role, with an output of around 50 kW. The CCHP device still did not produce any output. During low cold load hours, the output of all the devices was relatively low and similar, with the AC device having slightly a higher output than the other two devices; therefore, all three devices played a supporting role during low cold load hours.

During a 1–24 h period, the PES was charged at 14:00, 16:00, 18:00, 20:00, and 24:00, while discharge only occurred at 5:00, 17:00, 19:00, and 21:00. For the rest of the time, there were no charging or discharging operations. The battery energy changed significantly over this period, starting from 5.71 kWh, and dropping down to its lowest point of 1.33

kWh at 5:00–9:00; it then reached its highest level, of 9.21 kWh, at the 15th hour, before slightly decreasing again at 23:00–24:00. Overall, the PES had limited charging and discharging operations during this period, but the battery energy showed significant changes at different times.

As shown in Table 3, the total cost of Case 1 was CNY 12,017.8, and the cost for electricity, heat, cold, and PES were CNY 9266.0, 1560.2, 1184.3, and 7.4, respectively. In conclusion, the centralized energy management strategy applied to our PIES can enable efficient and coordinated utilization of electricity, cold, and heat, thus promoting environmental sustainability.

**Table 3.** Cost of Case 1.

| Node Type | Cost (CNY) |
|---|---|
| Electricity | 9266.0 |
| Heat | 1560.2 |
| Cold | 1184.3 |
| PES | 7.4 |
| Total | 12,017.8 |

### *4.2. Case 2: Distributed Energy Management for PIES on a Typical Summer Day*

In this case, we classified the nodes according to the type of devices, as shown in Figure 5, and then applied the proposed energy management strategy for our PIES on a summer typical day, including three electricity, three heat, three cold, and three PES nodes, respectively. The results of the dispatch plan for Case 2 are presented in Figure 6.

During the high electricity demand periods, such as from 8:00 to 18:00, the CCHP device had an output ranging from 18.58 kW to 142.28 kW, with its peak output at around 140.47 kW, between 11:00 and 13:00. Meanwhile, the EED's output fluctuated between 10.99 kW and 99.99 kW, showing a general upward trend during the day. The WT output slightly increased, peaking at no more than 89.47 kW during high demand hours. During low electricity demand periods, all the devices had lower output, with the CCHP device, the EED, and the WT all having outputs below 8.91 kW. Overall, the CCHP device was the main power generation device, playing a critical role in the overall operation of the system during peak demand periods.

During high heat demand periods, such as 1:00–5:00 and 16:00–20:00 hours, the EH device had the highest output values, reaching up to 91.38 kW and 73.97 kW, respectively, for the aforementioned periods. The GB device also had a small amount of output during some time periods, while the CCHP device remained idle. During low heat demand periods, such as 10:00–15:00 and 21:00–24:00, the output of all the devices was relatively low and unstable, with some hourly values being zero. In other time periods, the output of each device was relatively balanced, but the entire output of the EH device was still higher than that of the other devices. Overall, the EH device was the main power output device, and the GB device was an auxiliary power output device, while the CCHP device did not play a role.

During the high cold demand periods, which were 7:00–10:00 and 18:00–20:00, the output values of the EC device were the highest, reaching up to 68.47 kW and 71.76 kW, respectively, for the aforementioned periods. The AC device maintained a stable output of 50 kW, while the CCHP device remained idle. During the low heat demand periods, which were 1:00–6:00 and 21:00–24:00, all the device outputs were relatively low and unstable, with some hourly values being zero. In other time periods, the output of each device was relatively balanced; however, overall, the output of the EC device was still higher than that of the others. Therefore, we can conclude that the EC device provided the main power output during high demand periods, and that the AC device served as an auxiliary power output.

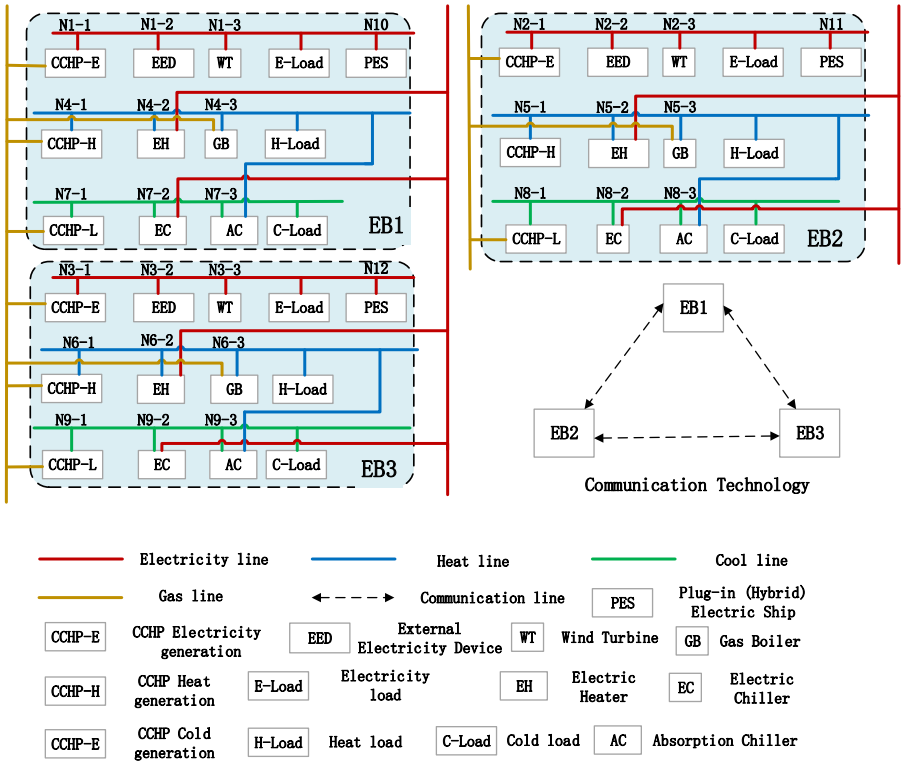


**Figure 5.** Node-specific classification.

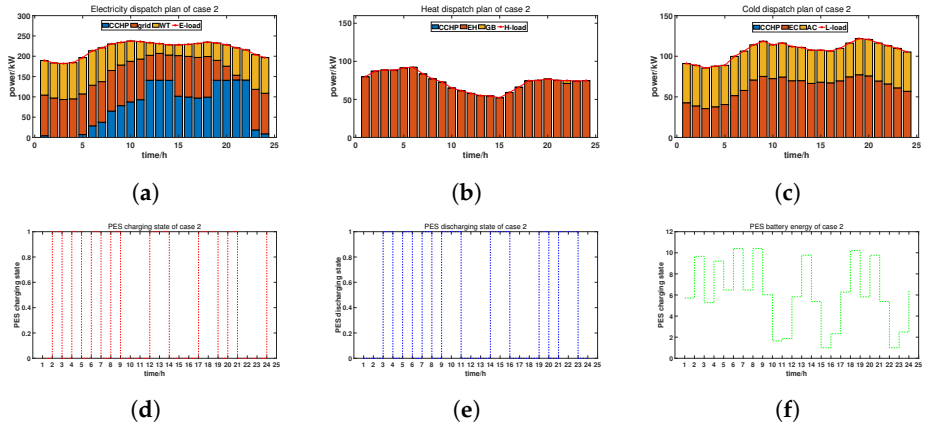


**Figure 6.** Dispatch plan of Case 2: (**a**) electricity dispatch plan; (**b**) heat dispatch plan; (**c**) cold dispatch plan; (**d**) PES charging state; (**e**) PES discharging state; (**f**) PES battery energy.

The PES charged at 2:00, 4:00, 6:00, 8:00, 12:00, 13:00, 17:00, 18:00, and 20:00. The PES discharged at 3:00, 5:00, 7:00, 9:00, 10:00, 14:00, 15:00, 19:00, 21:00, and 22:00. The PES battery energy level reached its peak at 15:00, with a value of 10.41 kWh, and experienced some fluctuations during the entire period, but the overall trend was upward, with a final value of 6.42 kWh.

When implementing a distributed energy management strategy, it is crucial to make cost corrections, to ensure an accurate estimation of the actual cost (the dual cost). As illustrated in Figure 7, the corrected cost (the better-estimated cost) was found to be closer to the actual cost (the dual cost). In practice, the dual cost was calculated to be CNY 11,028.7, while the estimated cost was CNY 11,376.8. Nevertheless, after making data corrections, a much better estimate of the cost was obtained, which amounted to CNY 11,016.3. Therefore, we recovered the original solution to the problem by the better estimate of the state vector. As shown in Table 4, the total cost of Case 2 was CNY 11,016.3, and the costs for electricity, heat, cold, and the PES were CNY 8426.8, 1545.2, 1062.0, and −17.6, respectively.

Our PIES energy management problem can be classified as a mixed integer linear programming problem with global coupling constraints. The optimization process involved different vectors of dual variables $\lambda_i(k), i = 1, \ldots, I$, which were generated by the various global coupling constraints. In order to investigate the change of these dual variables, a simulation was conducted for 1–10,000 iterations, and the results are presented in Figure 8. It can be seen that all the vectors of the dual variables converged to a consensus value at the end of the optimization process. We derived the optimal solutions and their corresponding dual variable values for our PIES energy management problem.

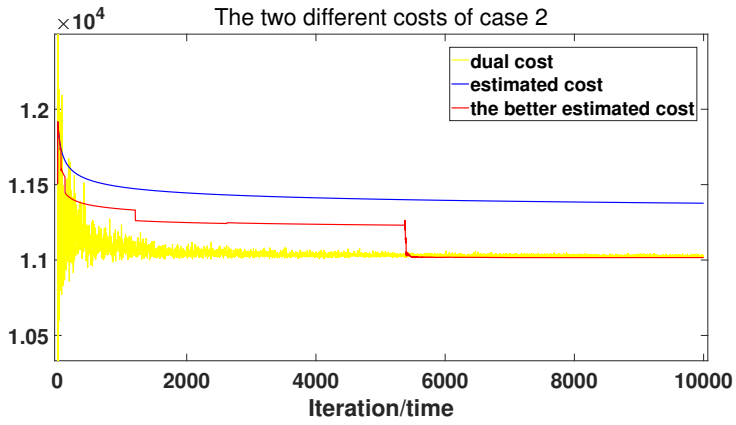


**Figure 7.** Total cost distance between Cases 1 and 2.

**Table 4.** Cost of Case 2.

| Node Type | Cost (CNY) |
|---|---|
| Electricity | 8426.8 |
| Heat | 1545.2 |
| Cold | 1062.0 |
| PES | −17.6 |
| Total | 11,016.3 |

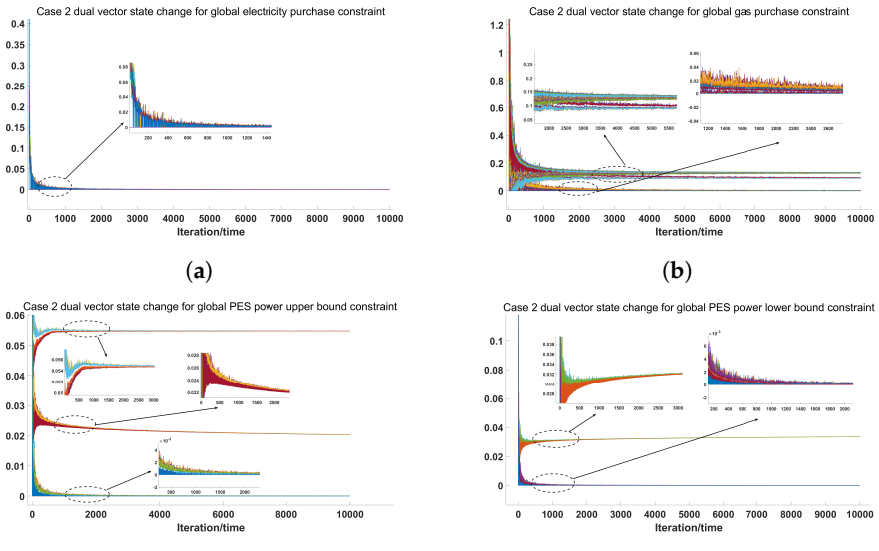


**Figure 8.** $\lambda_i(k), i = 1, \ldots, I$ for global constraints of Case 2: (**a**) $\lambda_i(k), i = 1, \ldots, I$ for global electricity purchase constraint; (**b**) $\lambda_i(k), i = 1, \ldots, I$ for global gas purchase constraint; (**c**) $\lambda_i(k), i = 1, \ldots, I$ for global PES power upper bound constraint; (**d**) $\lambda_i(k), i = 1, \ldots, I$ for global PES power lower bound constraint.

### 4.3. Case 3: Distributed Energy Management for PIES on a Typical Winter Day

This case applied the proposed energy management strategy to a typical winter day for our PIES. The dispatch plan for the different energy flows is shown in Figure 9.

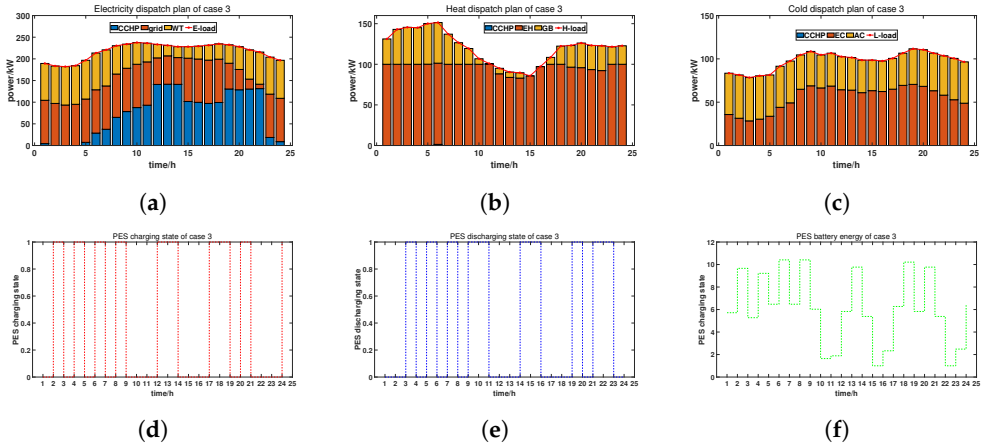


**Figure 9.** Dispatch plan of Case 3: (**a**) electricity dispatch plan; (**b**) heat dispatch plan; (**c**) cold dispatch plan; (**d**) PES charging state; (**e**) PES discharging state; (**f**) PES battery energy.

During the peak hours of electricity demand (5:00–12:00), the CCHP device's output was relatively stable, ranging from 28.6 kW to 92.9 kW. The WT output gradually increased during this period, peaking at 85.46 kW, indicating its role in providing additional support during the peak hours of electricity demand. On the other hand, the EED's output remained stable, at around 100 kW during the entire period, suggesting that EED played a crucial role in providing stable energy. During the off-peak hours of electricity demand (1:00–4:00 and 23:00–24:00), the CCHP device's output was low, sometimes even dropping to zero: this indicated that the CCHP device mainly provided additional electricity support during the peak hours of electricity demand. The WT output was also relatively low during this period, ranging from 25.2 kW to 50.1 kW, which may have been due to weak wind conditions and insufficient wind energy supply. However, the EED's output remained stable at around 100 kW during this period, indicating that it played an important role in providing stable base load electricity, regardless of electricity demand fluctuations.

The highest heat load period within 24 h occurred from 5:00–6:00: during this period, the CCHP device's output was very low, ranging from only 0.118 kW to 1.379 kW, while the EH device's output remained around 99.99 kW; the GB device's output peaked at about 50 kW from 5:00 to 6:00, and generally did not exceed 50 kW for the rest of the time. During periods of low heat load throughout the 24 h, the outputs of the CCHP device and of the GB device were generally low, often not exceeding 30 kW, while the EH device's output remained around 100 kW. Although the outputs of the CCHP, EH, and GB devices varied at different times, the EH device played the main role in generating stable energy throughout the 24-h period, while the GB device provided critical auxiliary heat support during peak periods. The CCHP device played a minor role in providing additional heat support during the peak period of high heat load.

The highest cold load occurred from 8:00 to 10:00. During this period, the CCHP device's output remained at around 0 kW, while the EC device's output remained between 28.5 kW and 61.6 kW, and the AC device's output remained stable at 50 kW. Therefore, during the peak of high cold load, the EC device played the main role in generating power, while the AC and CCHP devices play relatively minor roles. Throughout the 24-h period, there were times when the cold load was relatively low. During these periods, the power outputs of the CCHP and AC devices remained around 50 kW, while the EC device's output fluctuated between 27 kW and 41.5 kW: this indicated that, during the low period of cold load, the AC device was the primary power support device, while the CCHP and EC devices no longer played a significant role.

The PES alternated between charging and discharging during the 24-h period. Charging occurred at 1:00, 3:00, 5:00, 7:00, 9:00, 12:00, 13:00, 17:00, 18:00, and 20:00. Discharging occurred at 3:00, 5:00, 7:00, 9:00, 10:00, 14:00, 15:00, 19:00, 21:00, and 22:00. In addition, the battery energy level of the PES fluctuated continuously throughout the 24-h period, and the highest value was 10.41 kWh.

It can be seen from Figure 10 that all the vectors of the dual variables converged to a consensus value at the end of the optimization process. As shown in Table 5, the total cost of Case 3 was CNY 12,213.4, and the costs for electricity, heat, cold, and the PES were CNY 8468.6, 2811.1, 951.3, and −17.68, respectively.

Compared to Case 2, the cost of the heat node was higher, and the cost of the cold node was lower in Case 3, because the heat and cold loads varied in different seasons. The simulation results show that the proposed energy management strategy can be adapted to different weathers.

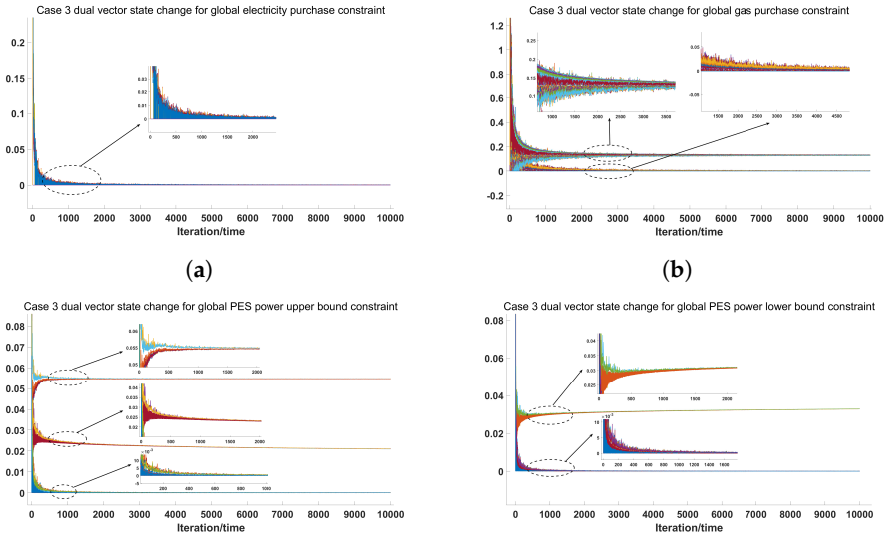


**Figure 10.** $\lambda_i(k), i = 1, \ldots, I$ for global constraints of Case 3: (**a**) $\lambda_i(k), i = 1, \ldots, I$ for global electricity purchase constraint; (**b**) $\lambda_i(k), i = 1, \ldots, I$ for global gas purchase constraint; (**c**) $\lambda_i(k), i = 1, \ldots, I$ for global PES power upper bound constraint; (**d**) $\lambda_i(k), i = 1, \ldots, I$ for global PES power lower bound constraint.

**Table 5.** Cost of Case 3.

| Node Type | Cost (CNY) |
|---|---|
| Electricity | 8468.6 |
| Heat | 2811.1 |
| Cold | 951.3 |
| PES | −17.68 |
| Total | 12,213.4 |

### *4.4. Case 4: Distributed Energy Management for PIES in Equipment Failure Scenario*

This case applied the proposed energy management strategy to our PIES with equipment failure, where the WT failed at 1:00–4:00. As in Case 3, this case applied to a typical winter day. The dispatch plan for the different energy flows is shown in Figure 11.

During the high electricity load periods, the CCHP device had a higher output value than the other two devices: specifically, between 8:00 and 20:00, the output value of the CCHP device remained above 80 kW, while the EED and the WT were below 60 kW. The maximum power value of the CCHP device occurred at 12:00, reaching 142.692 kW: this indicated that the CCHP device was the primary power generation device, and could provide more energy support during high electricity load. During the low electricity load

periods, the output values of all three devices were very low, but the output value of the WT was the highest. Between 12:00 and 18:00, the output value of the WT was around 50 kW. In summary, the CCHP device was the primary power generation device, and could provide more energy during high load periods, while the WT was the auxiliary power generation device, and could provide necessary energy support during low load periods.

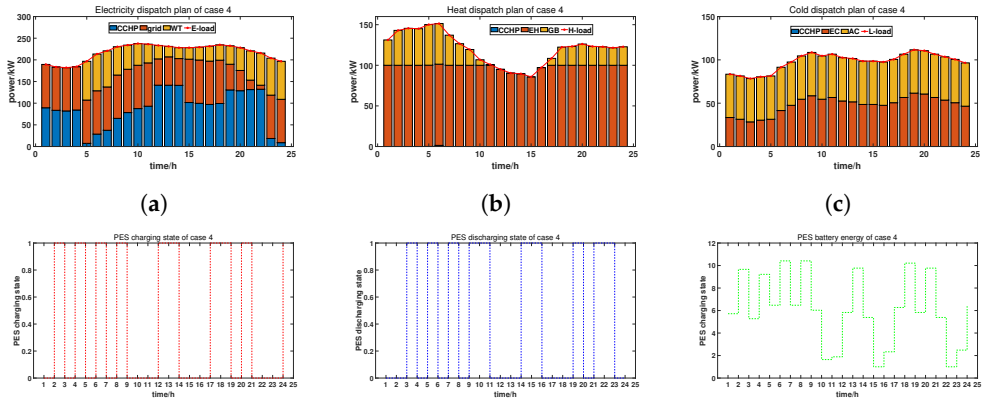


**Figure 11.** Dispatch plan of Case 4: (**a**) electricity dispatch plan; (**b**) heat dispatch plan; (**c**) cold dispatch plan; (**d**) PES charging state; (**e**) PES discharging state; (**f**) PES battery energy.

At high heat loads, the CCHP device's output values were highest at 5:00–6:00 and 16:00–18:00, at 0.11 kW and 1.37 kW, but its output value was 0 for the rest of the time. The output value of the EH device remained at 100.00 kW, and the GB device at its highest load also reached 50.00 kW, but remained below this value for the rest of the time, with no output from the GB device at all during hours 14:00–15:00. At low heat loads, the output values of the CCHP, EH, and GB devices were all lower than at high loads, but were relatively stable, with the output values of the CCHP and GB devices being 0 for most of the time, and the output value of the EH device remaining at 100.00 kW. The EH device was the main output device, always maintaining a output of 100.00 kW, while the CCHP and GB devices were auxiliary output devices, mainly providing some output at high loads.

During the peak cold load period (18:00–22:00), the EC device had the highest output power, ranging from 67.19 kW to 69.86 kW, while the AC device had a comparatively lower output power, ranging from 41.75 kW to 48.30 kW. The EC device was the primary power source during this time period, while the AC device's output power was relatively low. During the off-peak cold load period (4:00–7:00), the AC device had the highest output power, ranging from 47.02 kW to 48.30 kW, while the EC device had a comparatively lower output power, ranging from 42.31 kW to 45.74 kW. The AC device, therefore, played a major role in producing power during this time period, while the EC device's output power was relatively low.

The PES charged its battery during periods 2:00, 4:00, 6:00, 8:00, 12:00, 13:00, 17:00, 18:00, and 20:00, while discharging during periods 3:00, 5:00, 7:00, 9:00, 10:00, 14:00, 15:00, 19:00, 21:00, and 22:00. Over the 24-h period, the PES's battery energy level fluctuated between 1.64 kWh and 10.41 kWh.

Figure 12 shows that all the vectors of the dual variables converged to a consensus value at the end of the optimization process. As shown in Table 6, the total cost of Case 4 was CNY 13,158.1, and the costs for electricity, heat, cold, and PES were CNY 9363.4, 2808.6, 1003.7, and −17.7, respectively.

Compared to Case 3, the cost of Case 4 was significantly higher, due to the fact that in the case of the WT failure, the electricity and gas purchased by our PIES increased to meet different load demands. The simulation results show the benefits of incorporating renewable energy devices, indicating that PIESs can achieve stable and economical operation under the proposed energy management strategy.

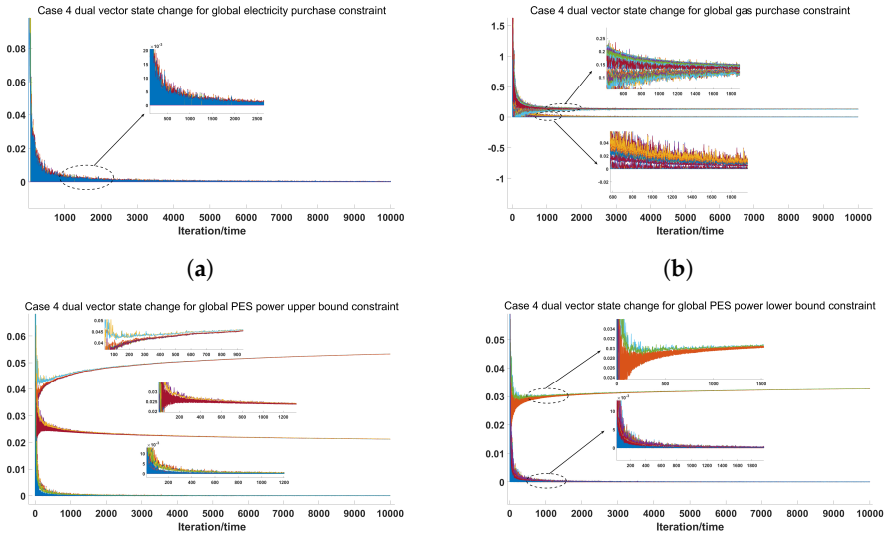


**Figure 12.** $\lambda_i(k), i = 1, \ldots, I$ for global constraints of Case 4: (**a**) $\lambda_i(k), i = 1, \ldots, I$ for global electricity purchase constraint; (**b**) $\lambda_i(k), i = 1, \ldots, I$ for global gas purchase constraint; (**c**) $\lambda_i(k), i = 1, \ldots, I$ for global PES power upper bound constraint; (**d**) $\lambda_i(k), i = 1, \ldots, I$ for global PES power lower bound constraint.

**Table 6.** Cost of Case 4.

| Node Type | Cost (CNY) |
|---|---|
| Electricity | 9363.4 |
| Heat | 2808.6 |
| Cold | 1003.7 |
| PES | −17.7 |
| Total | 13,158.1 |

### *4.5. Comparison of Cases*

In order to compare the results of the proposed energy management strategy in different scenarios to various numbers of nodes, simulations were carried out for different cases, and the results are shown in Table 7, which presents 12 instances of our PIES, each of which include information such as different scenarios, total node numbers, and the numbers of electricity, cold, heat, and PES nodes. Moreover, this table exhibits performance indicators, including centralized cost, distributed cost, and solving time in different instances. The data in this table reveal that different scenarios and node numbers affected the optimization results. The increase of node numbers led to a significant increase in the solving time for optimization problems. However, the gap between the distributed cost obtained by the distributed algorithm and the centralized cost obtained by the centralized algorithm decreased, because more available devices could be selected, with more nodes, prioritizing low-cost energy supply devices. Compared to the summer and winter scenarios, the equipment failure scenarios resulted in higher centralized costs and distributed costs: this highlights the importance of applying the WT in the PIES. Consequently, there existed complex mutual relationships among the node numbers, scenario types, and costs.

**Table 7.** Comparison of Cases.

| Instance | Scenario | Total Nodes | Electricity (Cold, Heat, PES) Nodes | Centralized Cost (CNY) | Distributed Cost (CNY) | Solve Time(s) |
|---|---|---|---|---|---|---|
| 1 | Summer | 12 | 3 (3,3,3) | 12,017.86 | 11,276.84 | 585.33 |
| 2 | Summer | 16 | 4 (4,4,4) | 11,115.38 | 10,576.48 | 877.37 |
| 3 | Summer | 20 | 5 (5,5,5) | 9552.81 | 9210.12 | 1087.3 |
| 4 | Summer | 40 | 10 (10,10,10) | 5580.09 | 5516.83 | 2145.37 |
| 5 | Winter | 12 | 3 (3,3,3) | 13,195.43 | 12,159.64 | 622.43 |
| 6 | Winter | 16 | 4 (4,4,4) | 10,199.46 | 9698.76 | 869.59 |
| 7 | Winter | 20 | 5 (5,5,5) | 8689.97 | 8373.6 | 1076.86 |
| 8 | Winter | 24 | 6 (6,6,6) | 7444.216 | 7180.15 | 1292.53 |
| 9 | Equipment Failure | 12 | 3 (3,3,3) | 14,153.09 | 13,057.49 | 611.28 |
| 10 | Equipment Failure | 16 | 4 (4,4,4) | 12,346.98 | 11,427.63 | 862.06 |
| 11 | Equipment Failure | 20 | 5 (5,5,5) | 10,837.61 | 10,008.43 | 1083.16 |
| 12 | Equipment Failure | 28 | 7 (7,7,7) | 8621.16 | 8044.36 | 1495.19 |

## 5. Conclusions

In this paper, we propose an energy management strategy based on distributed dual decomposition mixed integer linear programming for PIESs, to improve energy efficiency and foster green seaports. Taking into account the distributed characteristics presented by diverse heterogeneous devices, we established a PIES containing electricity replacement devices and energy conversion devices, based on a polymorphic network, to provide richer and more personalized services for PIESs. Taking into account the safety operation constraints and power balance constraints of seaports, we developed an energy management model for our PIES, to achieve economical and reliable operation for PIESs. Our proposed energy management strategy, based on distributed dual decomposition mixed integer linear programming, to solve the energy management problem of PIESs, distributed the coupling constraints equally to each node. Finally, we verified the effectiveness of the proposed energy management strategy, by simulation. The energy management problem solution obtained by our proposed distributed energy management strategy was close to the result obtained by the centralized algorithm. In the future, we will further explore smarter and greener distributed energy management strategies for achieving the sustainable development of seaports.

**Author Contributions:** F.T. and Q.Z. designed the study; Z.B. analyzed the data, and revised the manuscript; Q.Z. contributed to methodology development, and drafted the manuscript; G.X. provided software support, and participated in data analysis; Y.L. collected and curated the data; Y.G. assisted with data collection and analysis. All authors have read and approved the final manuscript.

**Funding:** This work was supported by the National Key Research and Development Project of China (Grant No. 2022YFB2901400), the National Natural Science Foundation of China (Grants No. U22A2005, 52201407, and 62203403), the High-Level Talents Innovation Support Plan of Dalian (Young Science and Technology Star Project) (Grant No. 2021RQ058), the Zhejiang Lab Open Research Project (Grant No. K2022QA0AB03), the Fundamental Research Funds for the Central Universities (Grant No. 3132023103), and the Key Research Project of Zhejiang Lab (Grant No. 2021LE0AC02).

**Institutional Review Board Statement:** Not applicable.

**Informed Consent Statement:** Not applicable.

**Data Availability Statement:** Not applicable.

**Acknowledgments:** Our thanks to the hard-working editors, and for valuable comments from the reviewers.

**Conflicts of Interest:** The authors declare no conflict of interest.

## Abbreviations

The following abbreviations are used in this manuscript:

| | |
|---|---|
| PIES | Port Integrated Energy System |
| CCHP | Combined Cooling, Heating, and Power |
| EH | Electric Heater |
| EC | Electric Chiller |
| EB | Energy Body |
| GB | Gas Boiler |
| AC | Absorption Chiller |
| PES | Plug-in Electric Ship |
| EED | External Electricity Device |
| WT | Wind Turbine |

## References


1. Acciaro, M.; Ghiara, H.; Cusano, M.I. Energy management in seaports: A new role for port authorities. *Energy Policy* **2014**, *71*, 4–12. [CrossRef]
2. Mianaei, P.K.; Aliahmadi, M.; Faghri, S.; Ensaf, M.; Ghasemi, A.; Abdoos, A.A. Chance-constrained programming for optimal scheduling of combined cooling, heating, and power-based microgrid coupled with flexible technologies. *Sustain. Cities Soc.* **2022**, *77*, 103502. [CrossRef]
3. Gao, J. Research on benefit evaluation method of integrated energy system considering the effect of electricity substitution. Ph.D. Thesis, North China Electric Power University, Beijing, China, 2021.
4. Iris, Ç.; Lam, J.S.L. A review of energy efficiency in ports: Operational strategies, technologies and energy management systems. *Renew. Sustain. Energy Rev.* **2019**, *112*, 170–182. [CrossRef]
5. Canbulat, O.; Aymelek, M.; Turan, O.; Boulougouris, E. An application of BBNs on the integrated energy efficiency of ship–port interface: A dry bulk shipping case. *Marit. Policy Manag.* **2019**, *46*, 845–865. [CrossRef]
6. Sifakis, N.; Kalaitzakis, K.; Tsoutsos, T. Integrating a novel smart control system for outdoor lighting infrastructures in ports. *Energy Convers. Manag.* **2021**, *246*, 114684. [CrossRef]
7. Iris, A.; Lam, J. Optimal energy management and operations planning in seaports with smart grid while harnessing renewable energy under uncertainty. *Omega* **2021**, *103*, 102445. [CrossRef]
8. Rolán, A.; Manteca, P.; Oktar, R.; Siano, P. Integration of cold ironing and renewable sources in the barcelona smart port. *IEEE Trans. Ind. Appl.* **2019**, *55*, 7198–7206. [CrossRef]
9. Wang, Y.; Liang, C.; Aktas, T.U.; Shi, J.; Pan, Y.; Fang, S.; Lim, G. Joint Voyage Planning and Onboard Energy Management of Hybrid Propulsion Ships. *J. Mar. Sci. Eng.* **2023**, *11*, 585. [CrossRef]
10. Bartolozzi, I.; Rizzi, F.; Frey, M. Are district heating systems and renewable energy sources always an environmental win-win solution? A life cycle assessment case study in Tuscany, Italy. *Renew. Sustain. Energy Rev.* **2017**, *80*, 408–420. [CrossRef]
11. Ameri, M.; Besharati, Z. Optimal design and operation of district heating and cooling networks with CCHP systems in a residential complex. *Energy Build.* **2016**, *110*, 135–148. [CrossRef]
12. Rafiei, M.; Boudjadar, J.; Khooban, M.H. Energy management of a zero-emission ferry boat with a fuel-cell-based hybrid energy system: Feasibility assessment. *IEEE Trans. Ind. Electron.* **2020**, *68*, 1739–1748. [CrossRef]
13. Hu, Y.; Li, D.; Sun, P.; Yi, P.; Wu, J. Polymorphic smart network: An open, flexible and universal architecture for future heterogeneous networks. *IEEE Trans. Netw. Sci. Eng.* **2020**, *7*, 2515–2525. [CrossRef]
14. Wang, Z.; Jiang, D.; Wang, F.; Lv, Z.; Nowak, R. A polymorphic heterogeneous security architecture for edge-enabled smart grids. *Sustain. Cities Soc.* **2021**, *67*, 102661. [CrossRef]
15. Hu, Y.; Yi, P.; Sun, P.; Wu, J. Research on a fully dimensionally definable polymorphic intelligent network system. *J. Commun.* **2019**, *40*, 1–12.
16. Yigit, K.; Acarkan, B. A new electrical energy management approach for ships using mixed energy sources to ensure sustainable port cities. *Sustain. Cities Soc.* **2018**, *40*, 126–135. [CrossRef]
17. Tawfik, M.; Shehata, A.S.; Hassan, A.A.; Kotb, M.A. Renewable solar and wind energies on buildings for green ports in Egypt. *Environ. Sci. Pollut. Res.* **2023**, *30*, 47602–47629. [CrossRef]
18. Kumar, N.; Panda, S.K. Smart High Power Charging Networks and Optimal Control Mechanism for Electric Ships. *IEEE Trans. Ind. Inform.* **2022**, *19*, 1476–1483. [CrossRef]
19. Ceballos-Santos, S.; Laso, J.; Ulloa, L.; Salmón, I.R.; Margallo, M.; Aldaco, R. Environmental performance of Cantabrian (Northern Spain) pelagic fisheries: Assessment of purse seine and minor art fleets under a life cycle approach. *Sci. Total Environ.* **2023**, *855*, 158884. [CrossRef]
20. Kermani, M.; Shirdare, E.; Parise, G.; Bongiorno, M.; Martirano, L. A Comprehensive Technoeconomic Solution for Demand Control in Ports: Energy Storage Systems Integration. *IEEE Trans. Ind. Appl.* **2022**, *58*, 1592–1601. [CrossRef]
21. Odoi-Yorke, F.; Owusu, J.J.; Atepor, L. Composite decision-making algorithms for optimisation of hybrid renewable energy systems: Port of Takoradi as a case study. *Energy Rep.* **2022**, *8*, 2131–2150. [CrossRef]
22. Wang, X.; Huang, W.; Wei, W.; Tai, N.; Li, R.; Huang, Y. Day-ahead optimal economic dispatching of integrated port energy systems considering hydrogen. *IEEE Trans. Ind. Appl.* **2021**, *58*, 2619–2629. [CrossRef]
23. Olivares, D.E.; Cañizares, C.A.; Kazerani, M. A centralized optimal energy management system for microgrids. In Proceedings of the 2011 IEEE Power and Energy Society General Meeting, Detroit, MI, USA, 24–28 July 2011; pp. 1–6.
24. Wu, Y.; Lau, V.K.; Tsang, D.H.; Qian, L.P.; Meng, L. Optimal energy scheduling for residential smart grid with centralized renewable energy source. *IEEE Syst. J.* **2013**, *8*, 562–576. [CrossRef]
25. Sahoo, B.; Routray, S.K.; Rout, P.K. A novel centralized energy management approach for power quality improvement. *Int. Trans. Electr. Energy Syst.* **2021**, *31*, e12582. [CrossRef]
26. Zhao, B.; Liu, X.; Song, A.; Chen, W.N.; Lai, K.K.; Zhang, J.; Deng, R.H. PRIMPSO: A Privacy-Preserving Multiagent Particle Swarm Optimization Algorithm. *IEEE Trans. Cybern.* **2022**, 1–14. [CrossRef] [PubMed]
27. Pourbabak, H.; Luo, J.; Chen, T.; Su, W. A novel consensus-based distributed algorithm for economic dispatch based on local estimation of power mismatch. *IEEE Trans. Smart Grid* **2017**, *9*, 5930–5942. [CrossRef]
28. Nedic, A.; Ozdaglar, A. Distributed subgradient methods for multi-agent optimization. *IEEE Trans. Autom. Control* **2009**, *54*, 48–61. [CrossRef]

29. Torkan, R.; Ilinca, A.; Ghorbanzadeh, M. A genetic algorithm optimization approach for smart energy management of microgrids. *Renew. Energy* **2022**, *197*, 852–863. [CrossRef]
30. Tsaousoglou, G.; Soumplis, P.; Efthymiopoulos, N.; Steriotis, K.; Kretsis, A.; Makris, P.; Kokkinos, P.; Varvarigos, E. Demand response as a service: Clearing multiple distribution-level markets. *IEEE Trans. Cloud Comput.* **2021**, *10*, 82–96. [CrossRef]
31. Couraud, B.; Robu, V.; Flynn, D.; Andoni, M.; Norbu, S.; Quinard, H. Real-time control of distributed batteries with blockchain-enabled market export commitments. *IEEE Trans. Sustain. Energy* **2021**, *13*, 579–591. [CrossRef]
32. Abaeifar, A.; Barati, H.; Tavakoli, A.R. Inertia-weight local-search-based TLBO algorithm for energy management in isolated micro-grids with renewable resources. *Int. J. Electr. Power Energy Syst.* **2022**, *137*, 107877. [CrossRef]
33. Bay, C.J.; Chintala, R.; Chinde, V.; King, J. Distributed model predictive control for coordinated, grid-interactive buildings. *Appl. Energy* **2022**, *312*, 118612. [CrossRef]
34. Moafi, M.; Ardeshiri, R.R.; Mudiyanselage, M.W.; Marzband, M.; Abusorrah, A.; Rawa, M.; Guerrero, J.M. Optimal coalition formation and maximum profit allocation for distributed energy resources in smart grids based on cooperative game theory. *Int. J. Electr. Power Energy Syst.* **2023**, *144*, 108492. [CrossRef]
35. Zhang, H.; Li, Y.; Gao, D.W.; Zhou, J. Distributed optimal energy management for energy internet. *IEEE Trans. Ind. Inform.* **2017**, *13*, 3081–3097. [CrossRef]
36. Zhang, Y.; Xiao, Y.; Shan, Q.; Li, T. Towards Lower Carbon Emissions: A Distributed Energy Management Strategy-Based Multi-Objective Optimization for the Seaport Integrated Energy System. *J. Mar. Sci. Eng.* **2023**, *11*, 681. [CrossRef]
37. Teng, F.; Zhang, Q.; Zou, T.; Zhu, J.; Tu, Y.; Feng, Q. Energy Management Strategy for Seaport Integrated Energy System under Polymorphic Network. *Sustainability* **2022**, *15*, 53. [CrossRef]
38. Falsone, A.; Margellos, K.; Garatti, S.; Prandini, M. Dual decomposition for multi-agent distributed optimization with coupling constraints. *Automatica* **2017**, *84*, 149–158. [CrossRef]
39. Kusakana, K. Operation cost minimization of photovoltaic–diesel–battery hybrid systems. *Energy* **2015**, *85*, 645–653. [CrossRef]
40. Wang, X.; Song, J.; Wu, Q.; Bao, Y.; Wang, Y. A novel bi-level programming model for structure sustainability optimization of passenger transport corridor. *PLoS ONE* **2022**, *17*, e0266013. [CrossRef]